Journal of Manufacturing Processes 56 (2020) 1211–1218

Contents lists available at ScienceDirect

Journal of Manufacturing Processes

journal homepage: www.elsevier.com/locate/manpro

Effect of the initial-flaw on crack-propagation in two-step cutting of monocrystalline sapphire

Hae-Sung Yoon[a], Suk Bum Kwon[b], Aditya Nagaraj[b], Sangkee Min[b,*]

[a] School of Aerospace and Mechanical Engineering, Korea Aerospace University, 76 Hanggongdaehak-ro, Deogyang-gu, Goyang-si, Gyeonggi-do, 10540, Republic of Korea
[b] Department of Mechanical Engineering, University of Wisconsin-Madison, 1513 University Avenue, Madison, WI, 53706, USA

ARTICLE INFO

Keywords:
Brittleness
Cracks
Diamond tools
Sapphire
Stresses
Ultra-precision machining

ABSTRACT

Though superior multifunctional performances of sapphire, heavy surface/subsurface damage during the process limit applications of the material. Many efforts have been made to improve the machinability of the material, by utilizing the ductile-regime cutting. Here, in addition to the efforts on control of material behavior, machining strategies consisting of aggressive rough cutting and fine finish cutting were utilized in the machining of sapphire to improve the process throughput. To achieve this goal, it is required to investigate the effects of existing flaws in materials because their shapes and size significantly influence crack propagation in subsequent cutting. Considering this, machining behavior of primary and subsequent cutting was analyzed in terms of cutting direction of each, and the effects of existing cracks were investigated with respect to the crystal orientation and stress at the ductile-brittle transition point. Experimental results showed that existing flaws distinctively influence the crack propagation in subsequent cutting; the ductile cutting regime varied up to about 2 times with the combination of different primary and subsequent cutting directions. Based on the experimental results, a two-step cutting was performed as a proof of concept to optimize the material removal rate.

1. Introduction

Advanced ceramics, such as sapphire or zirconia, have drawn great attention thanks to their superior multifunctional performances, *i.e.*, high level of hardness and chemical stability [1]. However, it is very difficult to machine these materials, as their brittleness usually causes lots of surface cracks and subsurface damage during machining [2]. To resolve the issue on the surface quality, ductile regime cutting has been investigated. Dominant material response during cutting can drastically change depending on process environments [3,4]. Many researchers have investigated to explain material behavior during the process, as well as to improve the process efficiency [5].

In light of this, material removal mechanisms and response to external forces were analyzed concerning material's crystallography via micro indentation with various loads [6] or scratching in different directions [7]. Also, ultra-precision orthogonal cutting experiments were performed to predict anisotropic machining behavior [8], and to identify crack initiation parameters on different crystal planes [9]. Among various efforts in the modeling of material behaviors, preliminary experimental results showed that the dominant material response could be predicted in terms of the stress intensity factor of the corresponding crystal plane, or crack opening plane [9,10].

These efforts lead to formulating a model to predict material behaviors during the process, and further to develop machining strategies to improve process throughput. To achieve these goals, it is required to consider the effects of existing flaws in materials, or subsurface damage, since their shapes and size significantly influence crack propagation [11]. For example, it was found that machining repeatedly in a single direction initiates cracks much easier due to the damage accumulating in the material [12]. Further, to develop practical machining strategies consisting of aggressive rough cutting and fine finish cutting, investigation on the effects of pre-machined cracks on subsequent cutting is necessary.

Many efforts have been made to analyze the subsurface damage in cutting via direct and indirect methods [13]. The focused ion beam (FIB) and transmission electron microscope (TEM) are one of the most common tools to directly observe subsurface damage [14,15]. Wang et al. investigated the subsurface damage in the scratching of sapphire by cross-sectioning the cutting area using FIB [16]. The cracks were formed associated with the crystal structure of the material and could reach the depth a few times more than the machining depth (a few microns). Suzuki et al. observed subsurface damage via TEM and

* Corresponding author at: Department of Mechanical Engineering, University of Wisconsin-Madison, Room 1039, 1513 University Avenue, Madison, WI, 53706, USA.
E-mail addresses: hsyoon7@kau.ac.kr (H.-S. Yoon), kwon47@wisc.edu (S.B. Kwon), anagaraj2@wisc.edu (A. Nagaraj), sangkee.min@wisc.edu (S. Min).

https://doi.org/10.1016/j.jmapro.2020.06.017
Received 11 February 2020; Received in revised form 5 May 2020; Accepted 9 June 2020

analyzed the dislocation layer in fixed-abrasive diamond wire slicing of silicon [15]. However, those FIB and TEM techniques usually take a lot of time and cost to assess cracks. On the other hand, as one of the indirect methods, Cheng and Wu used corrosive liquid (molten KOH) to enlarge and visualize subsurface cracks in micro-slot-grinding of sapphire [17]. Langan et al. analyzed Micro-Raman spectroscopy to analyze the residual stress in the laser-assisted machining of sapphire to evaluate the damage left on the surface [18]. But it is not straightforward yet to directly match the subsurface damage and level of the residual stress.

Furthermore, it is not easy to directly assess initial flaws or subsurface damage at this small scale. Particularly, in the ultra-precision orthogonal cutting, these damages are expected to range at about tens of nanometers [19], and it takes a lot of effort and time even in sample preparation for the measurement [20]. Thus, this research targets to study the effects of cracks in an indirect way, particularly through two-step cutting as mentioned above.

Therefore, with the aim of practical machining strategies, the effects of surface and subsurface damage on subsequent cutting behavior were investigated by applying various combinations of two-step cutting. Experimental configurations and the suggested two-step cutting strategy were discussed more in detail in the next section. Material behavior and stresses were then discussed with respect to the crystal orientation and distinctive crack morphologies. Two-step cutting as a proof of concept was performed to create a pocket with a crack-free surface with an improved material removal rate.

2. Effects of subsurface damage on subsequent cutting

An ultra-precision machine tool (ROBONANO α-0*i*B, FANUC Corp., Japan) was used to perform single-point orthogonal cutting on sapphire (produced by Czochralski technique, M.T.I Corp., U.S.A). A dynamometer (Type 9119AA1, KISTLER Instrument Corp., Switzerland) and multi-channel amplifier (Type 5080A, KISTLER Instrument Corp.) were used to capture cutting forces with a sampling frequency of 20,000 Hz, and a low pass filter was then applied to the signal with a cut-off frequency of 5000 Hz. Here, a nano-polycrystalline diamond tool (nose radius of 500 μm, customized, A.L.M.T. Corp., Japan) was used to scribe the sapphire workpiece.

The main scheme of this study is shown in Fig. 1 (a). In the beginning, the first cut, herein referred to as primary cutting, is performed to generate different amounts of subsurface damage by varying the depth of cut and crystal orientation. Cutting paths were designed to have a flat area in the middle with a constant depth and repeated in a transverse direction with a pitch of 15 μm, to generate surface/subsurface damage over the desired area. With the given tool nose radius and pitch, the flat area is supposed to have the R_z (peak-to-peak) value of about 56 nm. Then, additional cutting, herein referred to as subsequent cutting, is performed on the surface machined by primary cutting. The primitive goal of the subsequent cutting is to achieve fine surface quality by removing cracks that occurred in primary cutting.

To analyze the machinability in a single-step cutting, previous work [9] studied the critical depth of cut (CDC) – a depth of cut where the first significant crack occurs. Here, the maximum stress at the tool-tip is hypothesized to dominantly contribute to crack propagation. Seeing the preliminary study in the machining of zirconia [21], the position where cracks start to propagate and angle of cracks changes in terms of the geometric relationship between the tool-edge and crack-opening crystal plane. Also, in another preliminary study [10], even tools with different nose radius showed similar CDCs to each other, and the stresses in the cutting direction were maintained as a constant. Combining the given findings, depth of cut can be a reasonable parameter to describe cutting performance by reflecting the level of the stress, as well as the material removal rate.

Here, to analyze anisotropic machining behaviors, cutting/thrust forces and cutting area were considered together to calculate the stress in a specific direction. The stress required in crack propagation was estimated using stress intensity factor, K_I, and a function of the geometric relationship between the cutting direction and crystal structure of sapphire, Fig. 1 (b) and was calculated by Eq. (1) [22]:

$$K_I = \sigma\sqrt{\pi a} \bullet \cos^2\beta \tag{1}$$

where σ is the tensile stress calculated from the cutting/thrust forces and cutting area, a is the half-length of an initial flaw, and β is an angle that the stress direction forms with the normal direction of the flaw, Fig. 1 (c). The previous work assumed that initial flaws were just uniformly distributed in the material with the same size, and the machining behavior was analyzed with respect to the magnitude and direction of the resultant force and cutting area at the CDC. It could explain anisotropic machining characteristics in the experiments; the CDC of different cutting direction could be predicted in terms of the stress in a direction normal to the dominant crack-opening plane.

However, if the subsequent cutting is applied to the surface with damage from primary cutting, further analysis is required on factors influencing the stress intensity. Compared to the cutting on the original surface without primary cutting, material behavior in subsequent

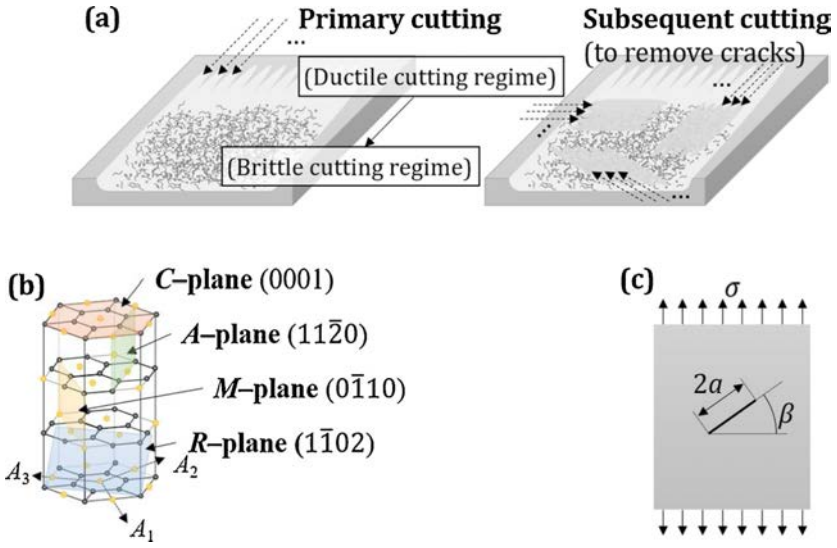

Fig. 1. (a) Schematic images of primary and subsequent cutting, (b) crystal structure and primary planes of sapphire [**8**], and (c) a scheme of crack opening with an initial flaw.

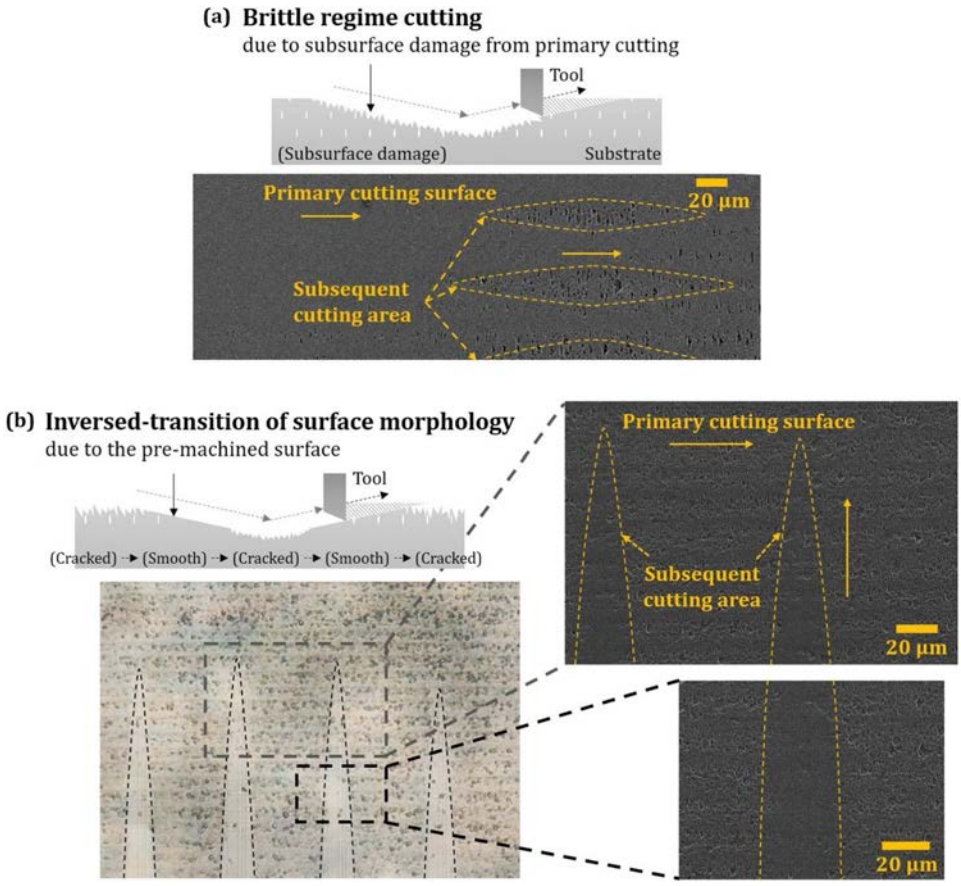

Fig. 2. Examples of the effects of primary cutting on subsequent cutting area (a) all brittle surface (primary cutting: [1$\bar{1}$01], subsequent cutting: [1$\bar{1}$01]), and (b) brittle-ductile-brittle surface (primary cutting: [1$\bar{1}$01], subsequent cutting: [11$\bar{2}$0]).

cutting may drastically change due to the surface and subsurface damage caused by primary cutting. As the direction and size of the flaw might change, combinations of primary and subsequent cutting will matter the machining characteristics as well.

Fig. 2 shows two representative cases showing the effect of the primary cutting on subsequent cutting. Here, subsequent cutting was designed to be a plunge cut with a slope of 1/500, to observe the transition of dominant material response during the cutting. If the direction of surface and subsurface damage by primary cutting are aligned with the crack opening direction in subsequent cutting, new cracks will easily propagate due to the pre-existing damage, enlarged flaw. In this case, the dominant material response of the subsequent cutting could be all brittle without ductile regime surface even if the surface from primary cutting seems to be smooth (Fig. 2 (a)). The same cutting direction of [1$\bar{1}$01] was used both for primary and subsequent cutting on the *R*-plane of sapphire.

On the other hand, if the depth of the cracks by primary cutting is small, the subsequent cutting may remove the damage while the entire subsequent cutting is done in ductile mode. Fig. 2 (b) shows cracked-smooth-cracked surfaces created by subsequent plunge cuts. Directions of primary and subsequent cutting were selected to be perpendicular to have different machining characteristics. At a shallow depth of cut, the subsequent cutting could remove only some part of the damage, because the size of damage from primary cutting is larger than the depth of the subsequent cutting. Hence, it remains as a cracked surface, though the subsequent cutting is done in the ductile regime in this region. Then it showed a smooth surface by fully removing cracks from primary cutting as the depth increases. If the depth of cut is getting deeper over the CDC of the subsequent cutting, it will create cracks again due to the brittle behavior in subsequent cutting.

Considering those cases mentioned above, to effectively remove cracks by a two-step cutting strategy, the depth of the damage that can be removed by the subsequent cutting should be less than the CDC of the subsequent cutting and the damage should not be aligned to likely direction of crack opening of the subsequent cutting. Therefore, it is very important to carefully choose the depth and direction of the primary cutting considering damage removal by the subsequent cutting. Thus, the effects of surface and subsurface damage were studied per various combinations of primary and subsequent cutting, regarding their size, morphology, and geometric orientation.

Detailed experimental configuration was explained in Section 3.1 with related terminologies. It is then followed by an analysis of the effects of the depth of primary cutting on the subsequent cutting. In Section 3.3, primary cutting in various directions was tested with the same subsequent cutting condition, while in Section 3.4, subsequent cutting in various directions was investigated with the same primary cutting condition. A two-step cutting strategy was proved by creating a pocket with a crack-free surface in Section 3.5.

3. Results and discussion

3.1. Experimental details and terminology

A basal plane of sapphire (*C*-plane) used for this experiment showed a three-fold symmetry following a hexagonal cell structure [8]. Considering this, four cutting directions, 0°- [11$\bar{2}$0], 30°- [10$\bar{1}$0], 60°- [2$\bar{1}$10], and 90°- [1$\bar{1}$00], were used here as representative directions. Table 1 shows detailed process parameters.

On the cracked surface area by primary cutting, subsequent plunge cut was then performed. Due to the slope of subsequent cutting, the

Table 1
Process parameters used in the experiments.

Items	Values
Feed rate	5 mm min^{-1}
Slope of plunge cut	1/500 (Rake angle: 0°)
Cutting directions	0°- [11$\bar{2}$0], 30°- [10$\bar{1}$0], 60°- [2$\bar{1}$10], and 90°- [1$\bar{1}$00] directions (on *C*-plane)

dominant material response changes depending on the depth of cut. Directions of primary and subsequent cutting may be either the same or different. To quantify the ductile regime of subsequent cutting, the CDC of subsequent cutting, herein referred to as modified-CDC, was measured, and compared with the CDC of primary cutting, or original-CDC. To measure original-CDCs, a plunge cut with the same slope of 1/500 was applied to the original substrate surface without preceding cutting. Original-CDCs vary in terms of cutting direction, and in this study, they range at about 150 nm–400 nm with the given tool and machining conditions. It may also vary with respect to detailed process parameters, such as tool edge radius, lubrication conditions, *etc*. Stresses at the ductile-brittle transition point were calculated in a similar manner and were referred to as modified- and original-stress, respectively. Subsequent cutting was repeated 3 times per direction and data were averaged.

Fig. 3 shows an example optical image of the cracked surface area (generated by cutting in [2$\bar{1}$10] direction) and a slot of subsequent plunge cutting in [11$\bar{2}$0] direction. Subsequent cutting could remove cracks from primary cutting in some regions; however, it showed brittle cutting behavior at a large depth of cut in the middle where the depth exceeds the modified-CDC. Forces in Fig. 3 also shows ductile to brittle transition corresponding to the surface morphology. Here, a low pass filter with a cut-off frequency of 500 Hz was applied to the signal to emphasize force behavior more in detail. In the ductile regime, both cutting (F_y) and thrust forces (F_z) are relatively stable, with small vibration mainly caused by cracked surface (generated by primary cutting in [2$\bar{1}$10] direction with a pitch of 15 μm). While in the brittle regime, both cutting and thrust forces fluctuate largely due to crack propagation in subsequent cutting. The fluctuation of forces in the brittle regime is much larger and more uneven than that in the ductile regime. To determine the CDC, cutting force signals were considered together with optical images.

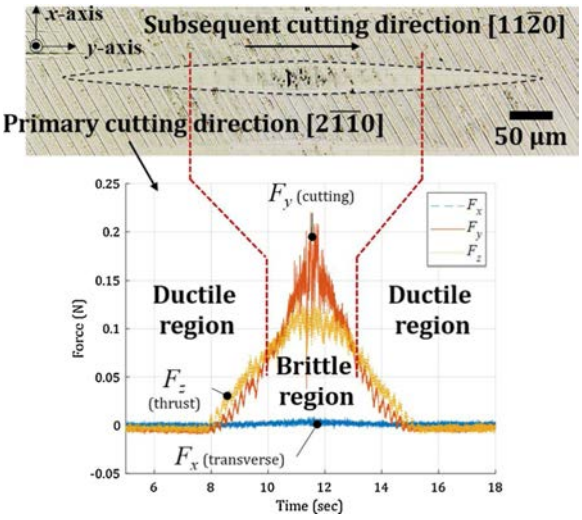

Fig. 3. An example of optical image and cutting force signal from subsequent cutting.

3.2. Effects of the depth of cut of the primary cutting

Fig. 4 shows modified-CDCs and stresses in terms of the depth of primary cutting. The depth of primary cutting varied from 150 nm to 350 nm while the depth of subsequent cutting was the same, in order to understand how primary cutting influences the CDC of the subsequent cutting. The subsequent plunge cutting was performed with a depth of 500 nm and modified-CDCs were measured per different depths of the primary cutting. Directions of primary and subsequent cutting are the same as 0°-direction, [11$\bar{2}$0]. When the depth of the generated surface is 150 nm in Fig. 4 (a), the modified-CDC is comparable to the original-CDC (without primary cutting, noted as a gray dotted line). It seems even slightly higher than the original-CDC but is still comparable to the range of variation. As the depth of the primary cutting increases, modified-CDC decreases due to enlarged flaws by primary cutting.

In Fig. 4 (b), modified-stresses are smaller than the original-stress overall (noted as a gray dotted line), and the average value ranged less than about 80 % of the original-stress. Because directions of primary and subsequent cutting are the same, it is obvious that cracks by primary cutting directly influences subsequent cutting, particularly due to increased length of flaws *a*, while any other geometric parameters remain the same (Eq. (1)). The critical stress intensity factor is assumed to be the same regardless of the existence of primary cutting as it is a material property depending on the thickness of the substrate [23]. Thus, the modified-stress decreases as the depth of cracked surface area increases due to enlarged *a*.

Hence, it can be inferred that primary cutting could lower the stress required to open the crack in the subsequent cutting and it reduced the ductile regime cutting by enlarging *a*. Residual stress left by primary cutting may influence on the subsequent cutting; however, considering that residual stresses are often relieved by chipping and cracks in the primary cutting [18], here the effect of the subsurface damage is thought to be more dominant on crack propagation in the subsequent cutting. Comparing to the trend of modified-stress, the cutting force in subsequent cutting should decrease more with reference to the depth of the primary cutting, to compensate for the effects of the reduced cutting area from the reduced modified-CDC.

3.3. Effects of the subsequent cutting direction

Fig. 5 shows CDC results for the primary cutting direction of 0°-, [11$\bar{2}$0], and subsequent cutting performed in 0°-, 30°-, 60°-, and 90°-directions. So that the subsequent cutting was performed in different directions on the cracked surface generated by the primary cutting of the same direction. The depth of the primary cutting was set to be 400 nm (original-CDC at [11$\bar{2}$0] direction: 228 nm) to generate enough cracks. Solid line with circular dots shows modified-CDCs, measured from the generated cracked surface, while the light gray dotted line with square dots shows original-CDCs measured from plunge cuts on the original substrate surface, with the purpose of comparison. Overall, modified-CDCs were about half of original-CDCs. The reduction of modified-CDC may be caused by the increased length of the flaw as mentioned above. It is not easy to categorize cracks' shapes in the subsequent cutting of four different directions, as their shapes are just similar to each other.

Among subsequent cutting, 30°-direction showed a slightly smaller CDC than 0°- or 60°-direction, while 90°-direction showed a relatively higher value. Primary cutting in 0°-direction dominantly initiates flaws in 30°-direction (*M*-plane normal (10$\bar{1}$0) direction) [9]. It then influences on crack initiation in the subsequent cutting of 30°-direction the most. Looking at the shape of cracks, it forms unique concave shapes, Fig. 5, due to the pile-up glide mechanism during plastic deformation (prismatic slip) [8]. Thus, the primary cutting also leaves propagated cracks at 30°-direction normal to 0°-direction and 60°-direction as indicated in the red box of Fig. 5. Tilted tiny cracks are seen on both lateral sides of the machined slots, and they influence the modified-

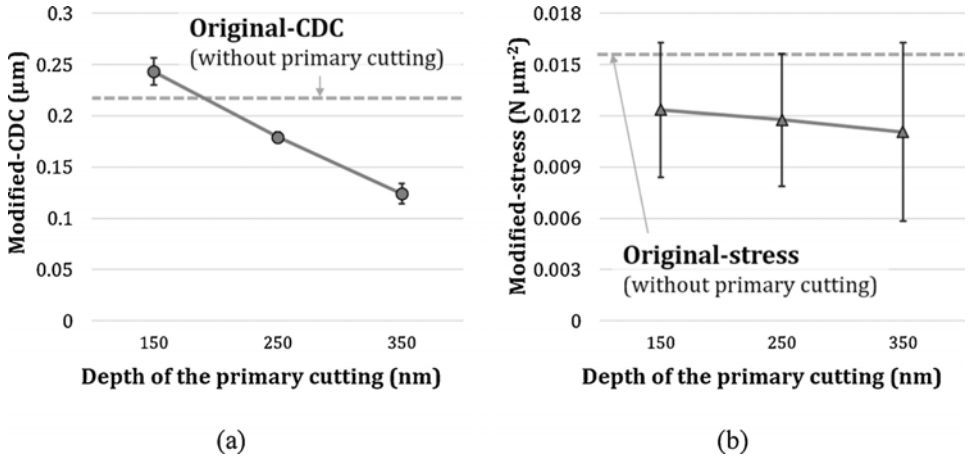

Fig. 4. Effects of the depth of cut of primary cutting on (a) modified-CDCs and (b) modified-stresses (primary and subsequent cutting direction: [11$\bar{2}$0]).

stresses of subsequent cutting in corresponding directions.

On the other hand, this anisotropic behavior might be overridden by the effects of surface shape generated by primary cutting, rather than surface/subsurface cracks. As the cracked surface is generated by the round tool (nose radius of 500 μm) with a pitch of 15 μm, the surface profile is supposed to have repetitive features with the R_z of 56 nm, theoretically. Here, the surface generated by primary cutting was measured using a white light interferometer (New View 6300, Zygo Corp., USA) and the roughness was calculated in a transverse direction to the primary cutting. The measured profile matched well with the designed pitch, and the R_z value ranged at about 100 − 120 nm including the cracks. However, the value itself is still smaller than most of the original- and modified-CDCs from the experiments, so it is thought that the surface morphology from the primary cutting is not dominant in cutting characteristics.

Fig. 6 shows the modified-stresses. As cracks propagated by the primary cutting are normal to 0°- or 60°-directions, stresses in those directions are smaller than that in 30°-direction, with a ratio of about $\cos^2 30°$ (Eq. (1)). On the other hand, modified-stress in 90°-direction showed a smaller value even than that in 30°-direction. In this direction, normal cracks to 0°-direction may contribute to lowering the stress.

Furthermore, in 90°-direction, surface and subsurface damage by primary cutting influence the dominant crack propagation mechanism. In 90°-direction cutting, [1$\bar{1}$00], on the surface without primary cutting, *M*-plane (($\bar{1}$100), the red arrow in Fig. 6 presents the normal direction of the plane.) influences crack opening [9], and the surface shows lamellar cracks normal to the cutting direction, Fig. 7 (a). However, in the subsequent cutting of the same direction on the cracked surface area, crack morphology changed to the concave shape, Fig. 7 (b), similar to cutting in 30°-direction. From the morphology, *R*-plane (1$\bar{1}$02) may influence crack opening. Unlike the case of the primary cutting, the thrust force in subsequent cutting could not enhanced the rhombohedral twinning in [1$\bar{1}$0$\bar{1}$] due to the damage caused by primary cutting, hence the ratio of the cutting force to thrust force largely decreased in subsequent cutting compared to the cutting without primary cutting.

3.4. Effects of the primary cutting direction

Meanwhile, Fig. 8 shows CDC results for subsequent cutting in 0°-direction, [11$\bar{2}$0], and primary cutting performed in 0°-, 30°-, 60°-, and 90°-directions. So here, four cracked surfaces were created by primary cutting in different directions, and on each cracked surface, the subsequent cutting was performed in the same direction [11$\bar{2}$0] to investigate the effect of primary cutting directions. Like the former set, the depth of primary cutting was set to be 400 nm. Cracks caused by subsequent cutting are mainly dotted cracks in all directions though the primary cutting in different directions created different types of cracks. As the original-CDC depends on cutting direction, the amount of subsurface damage also varies per cutting direction. Among different directions of the primary cutting, 0°-direction showed a smaller modified-CDC than that in other directions, while other directions showed similar values to the original-CDCs.

Except for 0°-direction, subsurface damage in other directions seems to be insufficient to influence ductile behavior in subsequent cutting. In subsequent cutting in [11$\bar{2}$0] direction, rhombohedral twinning in [01$\bar{1}\bar{1}$] (tilted downward following the red arrow in Fig. 8) is thought to dominate the ductile behavior, and the damage caused by primary cutting in 30°-, 60°-, and 90°-directions can effectively lower the force required in plastic deformation of subsequent cutting, which enables longer ductile regime in those directions rather than initiating cracks. Modified-CDC slightly increases then as the direction of primary cutting

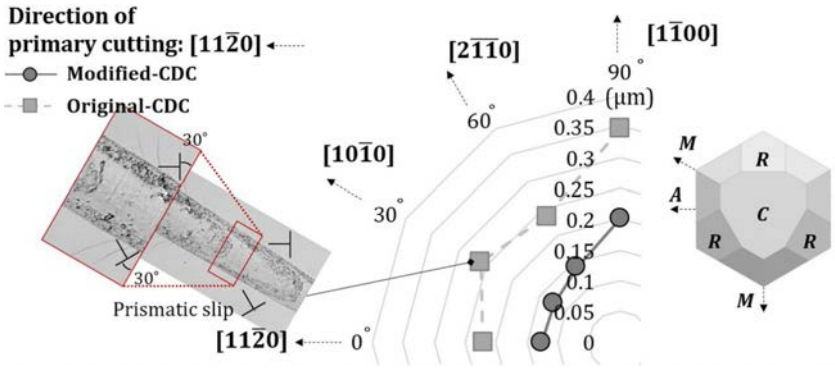

Fig. 5. Critical depth of cut (CDC) in terms of varying subsequent cutting directions.

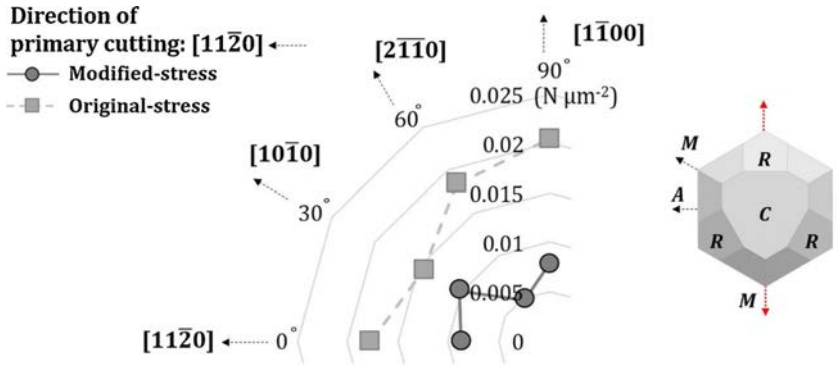

Fig. 6. Measured stress at the ductile-brittle transition point in terms of varying subsequent cutting directions.

changed from 30°- to 90°-direction. Nevertheless, though the small difference between modified- and original-CDCs showed in Fig. 8 and Fig. 9 shows that primary cutting significantly influences subsequent cutting in that modified-stresses are much smaller than the original value.

In addition, higher values of modified-CDC do not always guarantee a smooth surface in the subsequent cutting. In 90°-direction [1$\bar{1}$00], regardless of the depth of subsequent cutting, cracks generated by primary cutting was not fully removed due to its high depth. Fig. 10 shows that cracks are kept connected in the subsequent cutting area. Large subsurface damage by primary cutting also lowers the stress required for crack opening in the subsequent cutting, as shown in Fig. 9. Except for 90°-direction, the overall stress trend is similar to the former case, Fig. 6. Through the experimental results, it is shown that the effects of surface and subsurface damage could be explained with consideration of crack morphologies and the stress.

3.5 Example of two-step cutting strategy

Combining all the results, a simple experiment was performed to obtain a clean surface with improved process throughput. Fig. 11 shows a depth morphology of the machined pocket with a depth of cut of 500 nm, which was made by the primary cut of 350 nm in [11$\bar{2}$0] direction and subsequent cut of 150 nm (less than modified-CDC in Fig. 5) in [1$\bar{1}$00] direction. With the combination of the same cutting direction, it requires at least 3 times of repetitive cutting to make the clean surface, as preceding cutting keeps weakening the ductile cutting regime (original-CDC at [11$\bar{2}$0] direction: 228 nm).

Here, primary cutting of 0°-direction [11$\bar{2}$0] and subsequent cutting of 90°-direction [1$\bar{1}$00] were selected to achieve ductile cutting regime with a smooth surface. Then R_a value was measured and compared normal to the direction of cutting using surface profile data from the white light interferometer. Seeing the figure, cracks were clearly removed, and surface roughness of 0.950 nm was achieved from the cracked surface with a roughness of 25.3 nm, as well as with 1.5 times improvement in processing time (3 times of repetitive cutting vs. two-step cutting).

This result showed that machining strategies consisting of aggressive rough cutting and fine finish cutting could be successfully implemented and could improve the process throughput. In particular, the primary cutting may influence the CDC of the subsequent cutting regardless of the dominant material response in the primary cutting. Accumulated damage from preceding cutting lowers the level of the stress required to new crack opening and easily grow existing cracks. Thus, to improve the process throughput with the crack-free surface, an appropriate selection of depth of cuts for rough and finish cutting is necessary. Therefore, the effect of the initial flaw by the primary cutting needs to be carefully considered concerning the combination with subsequent cutting.

4. Conclusions

With the aim of two-step cutting strategies of improved process throughput, the effects of surface and subsurface damage on subsequent cutting were studied in the machining of single-crystal sapphire. With various combinations of primary and secondary cutting, machining characteristics were discussed and explained in terms of crack morphologies and geometric orientation. Size and orientation of flaws generated by primary cutting influenced the quality of machined surface produced in subsequent cutting by promoting the initiation of new cracks or removal of existing surface cracks. As the depth of primary cutting increased, modified-CDC and stress decreased due to an increase in the size of flaws which promoted crack initiation, reducing the ductile region. The amount of subsurface damage was dependent on the orientation of primary cutting whereas the orientation of subsequent cutting influenced the effect of subsurface damage on ductile material response. Based on the results, two-step cutting to create a pocket was successfully performed with higher productivity. Further, a comprehensive model will be developed to fully predict material behavior in the ceramic machining of complex steps. A strategy to optimize the process throughput with desired geometry will be investigated more in detail by varying the combination of aggressive rough and fine finish cutting.

Declaration of Competing Interest

The authors declare that they have no known competing financial interests or personal relationships that could have appeared to

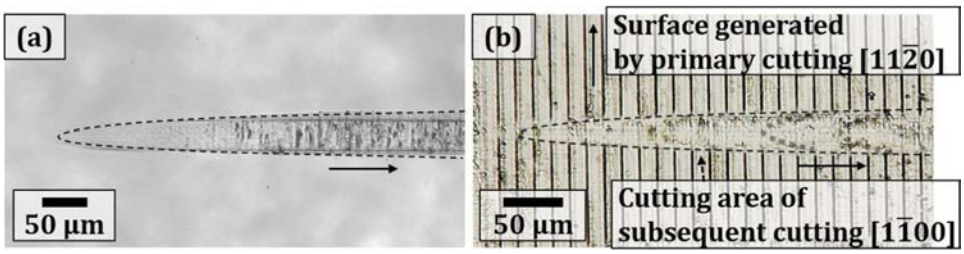

Fig. 7. A comparison of surface morphology in a cutting direction of [1$\bar{1}$00]. (a) without primary cutting, and (b) with primary cutting in [11$\bar{2}$0].

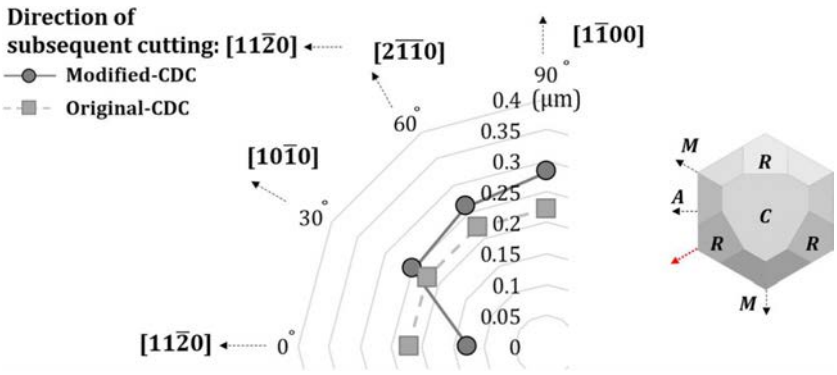

Fig. 8. CDC in terms of varying primary cutting directions.

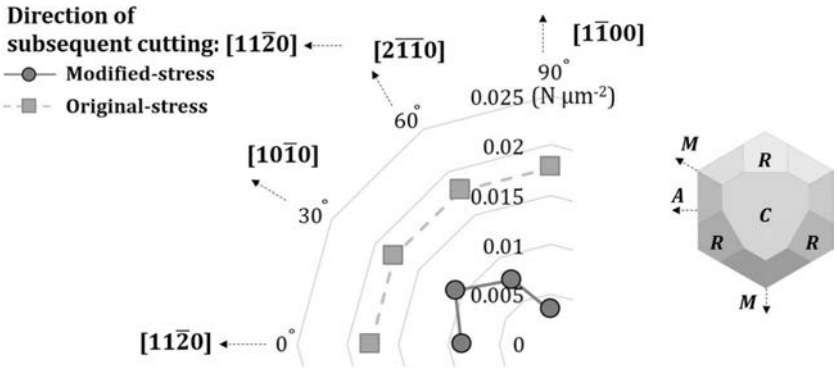

Fig. 9. Measured stress at the ductile-brittle transition point in terms of varying primary cutting directions.

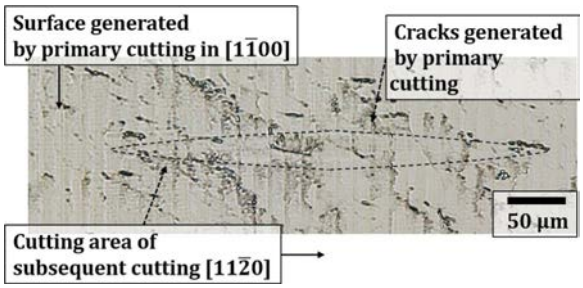

Fig. 10. Cracks left even after subsequent cutting.

influence the work reported in this paper.

Acknowledgements

This material is based on work supported by the NSF under grant No. CMMI-1844821. Authors gratefully acknowledge the use of facilities and instrumentation supported by NSF through the University of Wisconsin Materials Research Science Center (DMR-1720415) and kind support from FANUC Corporation, Japan, for the loan of 5- axis ultra-precision machine tool, ROBONANO α-0iB. The authors would also like to thank A.L.M.T. Corporation, Japan for providing the diamond tools used in this study. This work was also supported by the National Research Foundation of Korea (NRF) grant funded by Ministry of Science and ICT (No. NRF-2018R1C1B5085752), and 2018 KAU Faculty Research Grant.

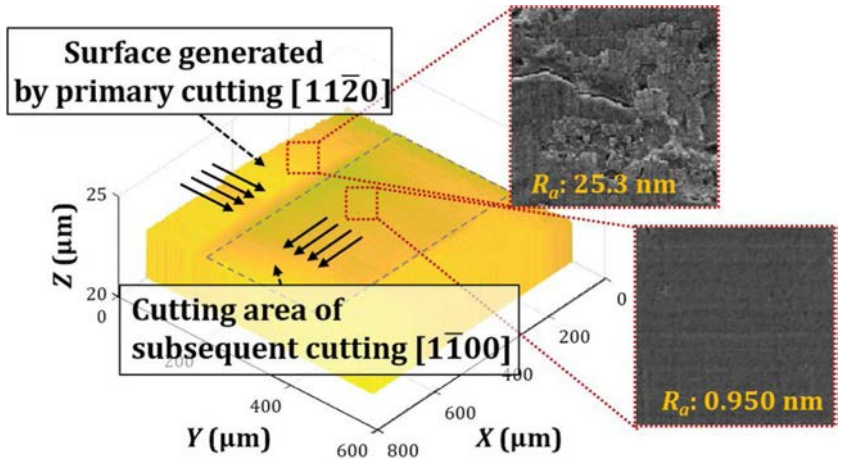

Fig. 11. Depth morphology of the surface created with improved process throughput (primary cutting: [11$\bar{2}$0], subsequent cutting: [1$\bar{1}$00].).

References

[1] Ferraris E, Vleugels J, Guo Y, Bourell D, Kruth JP, Lauwers B. Shaping of engineering ceramics by elecro, chemical and physical processes. CIRP Ann–Manuf Technol 2016;65(2):761–84. https://doi.org/10.1016/j.cirp.2016.06.001.

[2] Neo WK, Kumar AS, Rahman M. A review on the current research trends in ductile regime machining. Int J Adv Manuf Technol 2012;63(5–8):465–80. https://doi.org/10.1007/s00170-012-3949-y.

[3] Huang W, Yu D, Zhang X, Zhang M, Chen D. Ductile-regime machining model for ultrasonic elliptical vibration cutting of brittle materials. J Manuf Process 2018;36:68–76. https://doi.org/10.1016/j.jmapro.2018.09.029.

[4] Zhang J, Han L, Zhang J, Liu H, Yan Y, Sun T. Brittle-to-ductile transition in elliptical vibration-assisted diamond cutting of reaction-bonded silicon carbide. J Manuf Process 2019;45:670–81. https://doi.org/10.1016/j.jmapro.2019.08.005.

[5] Antwi EK, Liu K, Wang H. A review on ductile mode cutting of brittle materials. Front Mech Eng China 2018;13(2):251–63. https://doi.org/10.1007/s11465-018-0504-z.

[6] Wang K, Jiang F, Yan L, Xu X, Wang N, Zha X, et al. Study on mechanism of crack propagation of sapphire single crystals of four different orientations under impact load and static load. Ceram Int 2019;45(6):7359–75. https://doi.org/10.1016/j.ceramint.2019.01.021.

[7] Wang J, Guo B, Zhao Q, Zhang C, Zhang Q, Chen H, et al. Dependence of material removal on crystal orientation of sapphire under cross scratching. J Eur Ceram Soc 2017;37(6):2465–72. https://doi.org/10.1016/j.jeurceramsoc.2017.01.032.

[8] Mizumoto Y, Maas P, Kakinuma Y, Min S. Investigation of the cutting mechanisms and the anisotropic ductility of monocrystalline sapphire. CIRP Ann–Manuf Technol 2017;66(1):89–92. https://doi.org/10.1016/j.cirp.2017.04.018.

[9] Yoon H-S, Kwon SB, Nagaraj A, Min S. Study of stress intensity factor on the anisotropic machining behavior of single crystal sapphire. CIRP Ann–Manuf Technol 2018;67(1):125–8. https://doi.org/10.1016/j.cirp.2018.04.114.

[10] Yoon H-S, Kwon SB, Nagaraj A, Min S. Investigation of the ductile cutting behavior of monocrystalline yttria-stabilized zirconia during ultra-precision orthogonal cutting. Int J Precis Eng Manuf 2019;20(9):1475–84. https://doi.org/10.1007/s12541-019-00150-9.

[11] Liu Y, Li B, Wu C, Zheng Y. Simulation-based evaluation of surface micro-cracks and fracture toughness in high-speed grinding of silicon carbide ceramics. Int J Adv Manuf Tech 2016;86(1–4):799–808. https://doi.org/10.1007/s00170-015-8218-4.

[12] Nagaraj A, Kwon SB, Yoon H-S, Min S. Crack removal behavior in ultra-precision machining of sapphire. Procedia Manuf 2019;34:393–8. https://doi.org/10.1016/j.promfg.2019.06.183.

[13] Li HN, Yu TB, Zhu LD, Wang WS. Evaluation of grinding-induced subsurface damage in optical glass BK7. J Mater Process Tech 2016;229:785–94. https://doi.org/10.1016/j.jmatprotec.2015.11.003.

[14] Gupta A, Chen C-CA, Hsu H-W-W. Study on diamond wire wear, surface quality, and subsurface damage during multi-wire slicing of c-plane sapphire wafer. Int J Adv Manuf Technol 2019;100(2019):1801–14. https://doi.org/10.1007/s00170-018-2656-8.

[15] Suzuki T, Nishino Y, Yan J. Mechanisms of material removal and subsurface damage in fixed-abrasive diamond wire slicing of single-crystalline silicon. Precis Eng 2017;50:32–43. https://doi.org/10.1016/j.precisioneng.2017.04.011.

[16] Wang Y, Liang Z, Zhao W, Wang X, Wang H. Effect of ultrasonic elliptical vibration assistance on the surface layer defect of M-plane sapphire in microcutting process. Mater Des 2020:108755https://doi.org/10.1016/j.matdes.2020.108755. In press.

[17] Cheng J, Wu J. Experimental investigation of fracture behaviors and subsurface cracks in micro-slot-grinding of monocrystalline sapphire. J Mater Process Tech 2017;242:160–81. https://doi.org/10.1016/j.jmatprotec.2016.11.030.

[18] Langan SM, Ravindra D, Mann AB. Mitigation of damage during surface finishing of sapphire using laser-assisted machining. Precis Eng 2019;56:1–7. https://doi.org/10.1016/j.precisioneng.2018.08.012.

[19] Mizumoto Y, Amano H, Kangawa H, Harano K, Sumiya H, Kakinuma Y. On the improvement of subsurface quality of CaF_2 single crystal machined by boron-doped nano-polycrystalline diamond tools. Precis Eng 2018;52:73–83. https://doi.org/10.1016/j.precisioneng.2017.11.005.

[20] Li Z, Zhang F, Zhang Y, Luo X. Experimental investigation on the surface and subsurface damages characteristics and formation mechanisms in ultra-precision grinding of SiC. Int J Adv Manuf Technol 2017;92(5–8):2677–88. https://doi.org/10.1007/s00170-017-0267-4.

[21] Yoon H-S, Lee S, Min S. Investigation of ductile-brittle transition in machining of yttrium-stabilized zirconia (YSZ). Procedia Manuf 2018;26:446–53. https://doi.org/10.1016/j.promfg.2018.07.052.

[22] Tada H, Paris PC, Irwin GR. The stress analysis of cracks handbook. third edition New York, USA: ASME Press; 2000.

[23] Mouritz A. Introduction to aerospace materials. Cambridge, UK: Woodhead Publishing; 2012. p. 454–68.